Polydimethylsiloxane embedded mouse aorta *ex vivo* perfusion model: proof-of-concept study focusing on atherosclerosis

Xueya Wang
Marc P. Wolf
Rahel Bänziger Keel
Roman Lehner
Patrick R. Hunziker

Polydimethylsiloxane embedded mouse aorta *ex vivo* perfusion model: proof-of-concept study focusing on atherosclerosis

Xueya Wang,[a*] **Marc P. Wolf,**[a*] **Rahel Bänziger Keel,**[a] **Roman Lehner,**[a] **and Patrick R. Hunziker**[a,b]
[a]University Hospital Basel, Nanomedicine Group, Clinic for Intensive Care, Petersgraben 4, CH-4031 Basel, Switzerland
[b]CLINAM Foundation for Nanomedicine, Basel, Switzerland

Abstract. Existing mouse artery *ex vivo* perfusion models have utilized arteries such as carotid, uterine, and mesenteric arteries, but not the aorta. However, the aorta is the principal vessel analyzed for atherosclerosis studies *in vivo*. We have devised a mouse aorta *ex vivo* perfusion model that can bridge this gap. Aortas from apoE$^{(-/-)}$ mice are embedded in a transparent, gas-permeable, and elastic polymer matrix [polydimethylsiloxane (PDMS)] and artificially perfused with cell culture medium under cell culture conditions. After 24 h of artificial *ex vivo* perfusion, no evidence of cellular apoptosis is detected. Utilizing a standard confocal microscope, it is possible to image specific receptor targeting of cells in atherosclerotic plaques during 24 h. Imaging motion artifacts are minimal due to the polymer matrix embedding. Re-embedding of the aorta enables tissue sectioning and immuno-histochemical analysis. The *ex vivo* data are validated by comparison with *in vivo* experiments. This model can save animal lives via production of multiple endpoints in a single experiment, is easy to apply, and enables straightforward comparability with pre-existing atherosclerosis *in vivo* data. It is suited to investigate atherosclerotic disease in particular and vascular biology in general. © *2012 Society of Photo-Optical Instrumentation Engineers (SPIE).* [DOI: 10.1117/1.JBO.17.7.076006]

Keywords: mouse; aorta; atherosclerosis; imaging; macrophages; *ex vivo*; time-lapse; confocal.

Paper 12078 received Feb. 6, 2012; revised manuscript received May 23, 2012; accepted for publication Jun. 1, 2012; published online Jul. 6, 2012.

1 Introduction

Atherosclerosis is the major cause of death in industrialized countries and is expected to be the major cause worldwide in the coming years.[1,2] The knowledge about pathophysiological mechanisms of the disease onset and progression has been substantially furthered in the past few years. Nowadays, it is understood that the formation of atherosclerotic plaques is an active inflammatory process, involving functions and cells of the immune system both on a local and systemic level, and is initiated at regions with disturbed blood flow.[3–6]

In order to further our understanding of biological processes in general, and more particularly of vascular biology, pathophysiology, and pharmacology, a variety of models are currently at hand. On an increasing complexity scale, these can consist of cell monocultures, cell co-cultures, three-dimensional cell (co-) cultures, organotypic cultures, *ex vivo* organ models, or *in vivo* models (mostly murine). Classical (i.e., one parameter endpoint per animal after sacrificing) mouse *in vivo* models of vascular disease, such as apoE$^{(-/-)}$[7] or LDL$^{-/-}$ for atherosclerosis, offer high complexity. However, each endpoint (*en face* analysis, histology) is represented by the sacrificing of at least one animal. Taking into account animal breeding and sample preparation (dissection, fixation, embedding, sectioning, and staining), multiple endpoint generation is time-consuming and labor-intensive. Also, from an ethical point of view, it is desirable to reduce the number of animals to be sacrificed to

a minimum. The *ex vivo* perfusion of viable blood vessels integrates the strengths of the *in vivo* and cell culture models. While it preserves most of the biological complexity of (diseased) vascular tissue, it offers a high level of experimental control and monitoring. More precisely, this means exact control of the perfusate composition and the ability to change it rapidly in order to test the dynamic responses of subsets of cells. The monitoring can be done in three dimensions (3D) with a temporal resolution down to the millisecond range using confocal (or two-photon) microscopy. With experimental durations of up to days, this can generate a multitude of "endpoints" that would not be achievable by means of classical *in vivo* experiments. This means a dramatic reduction of time, labor, and the number of animals to be sacrificed. Continuous microscopic observation over days (time-lapse) is crucial when studying the atherosclerotic disease progression or regression upon treatment. Significant changes in plaque biology are expected to occur within days in mice (corresponding to months in humans).[8] For *ex vivo* perfusion studies, mainly mouse arteries have been used, as their small dimensions allow microscopic observation over their entire cross-section, and the use of mouse models of atherosclerosis is widespread. Various approaches thereof have been presented utilizing imaging methods such as wide-field fluorescence microscopy,[9] confocal microscopy,[10] or two-photon microscopy.[10,11] Segments from carotid,[9–11] mesenteric,[11] or uterine[11] arteries have been used that were ligated to two glass pipettes and immersed in cell culture medium.

Historically, in classical mouse *in vivo* atherosclerosis research, only the aortic lesions have been analyzed, using either serial cross-sectioning or *en face* analysis. Therefore, a vast

---

*These authors contributed equally to this work.

Address all correspondence to: Xueya Wang, Nanomedicine Group, Clinic for Intensive Care, University Hospital Basel, Petersgraben 4, CH-4031 Basel, Switzerland. Tel:+41 (0)61 265 52 57; Fax:+41 (0)61 265 53 00; E-mail: wangxu@uhbs.ch

body of evidence on these lesions exists. However, these data cannot be directly compared to current *ex vivo* models, due to artery-specific biology of the plaques.[12,13] In order to bridge this gap, we herewith present a novel PDMS embedded mouse aorta *ex vivo* perfusion model that allows continuous 3D microscopic observation of mouse aortas, utilizing a standard confocal microscope. Moreover, the higher number and larger size of aortic lesions (including different stages in one sample), as compared to carotid arteries, produces statistically more relevant data in one experiment and further reduces the number of animals required. The employed embedding in a transparent, biocompatible, gas-permeable, and elastic polymer matrix [polydimethylsiloxane (PDMS)] enables optical imaging and gas exchange (oxygen[14] and CO_2[15]) and reduces imaging motion artifacts. Moreover, the numerous side branches of the aorta (i.e., 24 intercostal arterial branches), which would lead to leaking if the vessel were freely suspended in cell culture medium (as has been done with carotid artery segments without branches), become occluded in PDMS. PDMS is a polymer widely used in the life sciences. As a proof-of-concept, we use aptamer-Cy5 to stain macrophages in atherosclerotic plaques.

2 Materials and Methods

2.1 Animals

All mice used in this study were kept under specific pathogen-free conditions and in accordance with Swiss federal regulations. To establish a murine aortic *ex vivo* model, apolipoprotein E (apoE$^{(-/-)}$)-deficient mice (The Jackson Laboratory, Bar Harbor, Maine) and C57BL/6 wild-type mice were used. All experiments were carried out at 20 to 30 weeks of age. Mice were fed a chow diet, and apoE$^{(-/-)}$ mice were fed with a Western diet containing 21% fat supplemented with 1.25% cholesterol (2481, NAFAG, Switzerland) for five weeks from 10 weeks of age on to accelerate plaque formation, followed by a chow diet until experiments were performed.

2.2 PDMS Embedding

A mouse was euthanized with 30 mg/kg pentobarbital, and its vasculature was perfused with room temperature phosphate buffered saline (PBS) via cannulation of the left ventricle until blood was no longer visible in the perfusate. During section, the micro-catheters (5069, Medex, UK) were *in situ* inserted into the mouse aorta from both sides (into the aortic sinus through the left heart ventricle and into the abdominal aorta), glued (Histoacryl®, Braun Aesculap, Germany), and ligated together with surgical thread (Ethicon Prolene 3-0, Johnson & Johnson Medical GmbH, Germany). Then the aorta was extracted and dissected free of surrounding fat tissue under the binocular, as it would interfere with microscopical imaging due to additional light scattering and the increased distance of the atherosclerotic plaques from the microscope objective. The whole process was done in ice-cold DMEM medium (Invitrogen, Grand Island, NY). The branches of the aortic arch (innominate artery, left common carotid, and left subclavian artery) were occluded with tissue glue. Subsequently, the aorta-catheters ensemble was embedded in partially polymerized [polydimethylsiloxane (PDMS), Sylgard® 184, 1673921, Dow Corning, USA] and incubated at 37°C for 2 h until the PDMS polymerized sufficiently for further handling.

2.3 Perfusion System

The circulation system that was employed to perfuse the aortas consisted of a pump (peristaltic pump: Control Company, USA; syringe pump: Infusion Pumps—Fresenius Kabi, 018020, Germany), standard medical care tubing (pyrogen free), and a warming plate to warm the perfusate before reaching the aorta in order to mimic *in vivo* conditions. Optionally, for long-term experiments (more than 24 h), the perfusate can be constantly refreshed with medium by a syringe pump and a drain for used medium that are both connected to the circulation (Fig. 1). The drain comprises a standard 0.22 μm syringe filter to avert bacterial contamination of the circulating medium. The speed level of the peristaltic pump was set accordingly to
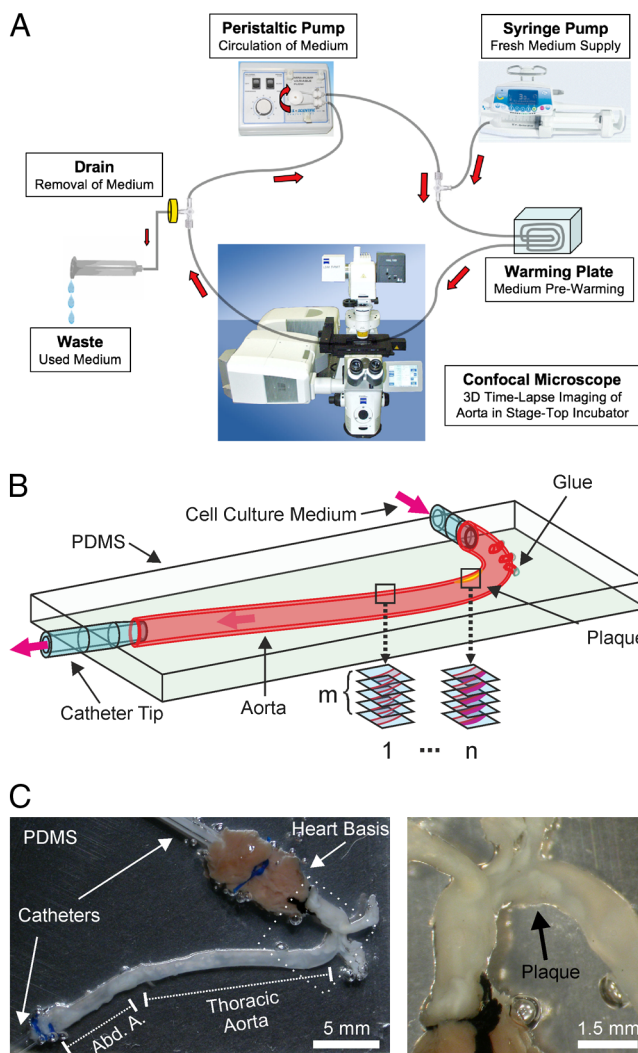

Fig. 1 System overview. (a) Schematic representation of the circulation system for the continuous perfusion of the embedded mouse aorta, consisting of the peristaltic pump, a warming plate, and the confocal microscope with stage-top incubator. (b) Schematic representation that shows the aorta connected to two catheters, embedded in PDMS, and perfused with cell culture medium. The basis of the heart is not depicted for clarity. Side branches of the aortic arch are ligated with tissue glue. Confocal imaging is possible with *m* slices on *n* positions with or without plaque. (c) Left, photograph of the connected aorta, including the basis of the heart, ligated with thread to two catheter tips. Abd. A.: abdominal aorta. Right: photograph of the aortic arch, with visible plaques at the lesser curvature of the aortic arch.

reproduce the physiological mean flow rate of the abdominal aorta in resting mice.[16] Oxygen supply and CO_2 clearance of the aortic tissue were allowed by passive diffusion through the surrounding PDMS.[14,15] For experiments, the embedded aorta was enclosed either in a conventional cell culture incubator (37℃, 5% CO_2, humidified) or in the stage-top incubation chamber of a Zeiss LSM710 confocal microscope (37℃, 5% CO_2, humidified).

2.4 Two-Photon Microscopy

Two-photon microscopy was performed on a Leica SP5 microscope (Leica Mikrosysteme, Wetzlar, Germany) with TiSa-Laser excitation at 850 nm.

2.5 Histology

Following time-lapse experiments, aortas were washed with PBS and fixed with 4% paraformaldehyde. The aortas were re-embedded in OCT (4583, Tissue-Tek, Medite, Germany), frozen down, and cryo-sectioned. Quantification of histological data was performed on 8 μm cryosections. In addition to standard hematoxylin-eosin staining, elastic fibers were stained using Elastin van Gieson (EvG) staining also named Verhoeff-van Gieson]. Lipid deposition was analyzed with Bodipy 493/503 (D-3922, Molecular Probes) staining. Leukocytes were detected using antibodies against CD45.2 (109804, BioLegend). A VCAM-1 (vascular cell adhesion molecule 1) antibody (109804, BioLegend) was used to visualize the endothelium. Apoptotic cells were detected using a caspase-3 antibody (9664s, Cell Signalling). Frozen tissue sections were fixed in 4% paraformaldehyde for 10 min, and nonspecific binding sites were blocked for 30 min with PBS containing 3% bovine serum albumin (BSA) and 0.1% Tween-20. Sections were incubated with the first and secondary antibodies in PBS containing 1% BSA. Between the steps, slides were washed with PBS. Images were acquired using an Olympus BX61 microscope (Olympus Europa Holding GmbH, Hamburg, Germany) equipped with ColorView and F-View cameras. Image

acquisition settings were unchanged over the whole experiment. Digital images were acquired using the imaging software Cell^P (Olympus Imaging Europa GmbH, Hamburg, Germany) and processed using Adobe Photoshop.

2.6 Necropsy and Organ Embedding

For comparison of the *ex vivo* results with *in vivo* conditions, apoE$^{(-/-)}$ mice were intravenously injected with Cy5-conjugated aptamer. Mice were intraperitoneally euthanized with 30 mg/kg of pentobarbital and then perfused with 15 mL of pre-warmed PBS followed by 30 mL of 2% paraformaldehyde. Subsequently, the heart and aorta were removed and incubated in 2% paraformaldehyde for 2 h, rinsed twice in PBS, and equilibrated in 30% sucrose-PBS (wt/vol) overnight. Tissues were embedded in OCT compound and snap frozen at −70℃. Frozen samples were stored at −70℃ until further use. Tissue sections of 8 μm were cut with a cryotome (HM560, Microm International GmbH, Germany) on to Superfrost® plus glass slides (J1800AMNZ, Thermo Scientific, Menzel GmbH & Co. KG, Braunschweig, Germany). Sections were air dried for 30 min and either stained immediately or stored at −70℃ until further use.

3 Results

3.1 Aortic Tissue Viability

In a first step, we studied the viability of the aortic tissue after artificial perfusion. The PDMS-embedded aorta was enclosed in a cell culture incubator and perfused with cell culture medium using the peristaltic pump. After 24 h of perfusion, the aorta was fixed by perfusion of 4% paraformaldehyde, extracted from the PDMS block, re-embedded in OCT, cryo-sectioned, and stained. Eight cryo-sections are shown in Fig. 2. The first line corresponds to the aorta that was perfused for 24 h, while the second line shows an aorta that was fixed directly after harvesting. The four different stainings that were applied were hematoxylin and eosin (H&E), EvG, caspase-3, and VCAM-1 (vascular cellular adhesion molecule 1).
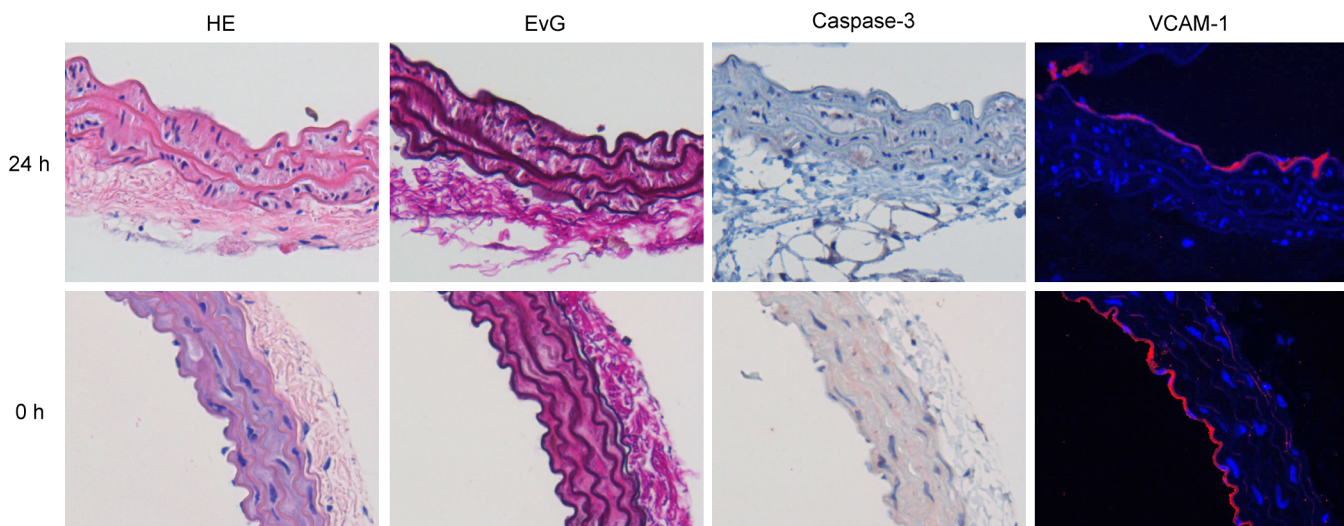

Fig. 2 Tissue viability assays. Aortic wall sections of aortas that were either perfused for 24 h with cell culture medium or directly processed after harvesting as a control (0 h). HE: Hematoxily-eosin staining shows the tissue structure. EvG: Elastin van Gieson shows the structure of elastin fibers (dark) and collagen fibers (pink). Caspase-3 staining is negative (i.e., no red dots), which precludes the presence of apoptosis. VCAM-1 staining (red fluorescent signal) stains activated endothelial surface (nuclei are stained blue). The continuous red lining proves the intactness of the endothelial layer.

The H&E staining is broadly used to visualize histo-morphology. It stains the cell nuclei blue and the (eosinophilic) cytoplasm and collagen pink. In the H&E staining, the perfused and nonperfused aorta sections are histo-morphologically similar. The collagen layers and the smooth muscle cells are intact (i.e., there is no sign of mechanical damage or necrosis). The EvG staining is generally used to stain extra-cellular matrix components, such as collagen and elastin fibers. Discontinuity of these fibers can be a sign of tissue necrosis. In the EvG staining, the perfused and nonperfused aorta sections show no discontinuities of collagen or elastin fibers. This precludes tissue necrosis. The caspase-3 staining is used as an indicator of apoptosis (programmed cell death). In the caspase-3 staining, neither the perfused nor the nonperfused aorta sections indicate signs of apoptosis. VCAM-1 is a mediator of endothelial leukocyte adhesion and is present on activated endothelium (i.e., in regions with disturbed flow), which includes endothelium on and around atherosclerotic lesions.[17] The VCAM-1 staining can be used as an indicator of endothelial cell layer integrity. As shown in Fig. 2, the VCAM-1 staining produces a red fluorescent lining on the luminal margin, corresponding to VCAM-1 presence on the luminal endothelial cell surface (nuclei are stained blue). The spatial continuity of the VCAM-1 signal confirms the intactness of the endothelial cell layer. However, the VCAM-1 fluorescence signal from the perfused aorta is less intense than the signal from the nonperfused aorta. This could be an indication of endothelial stress that could be attributable to mechanical handling, 2 h of incubation without perfusion during PDMS polymerization, or perfusion of cell culture medium. Endothelial cells are very sensitive to mechanical damage (e.g., due to specimen handling) and to their chemical environment (e.g., composition of the perfusate).

These data demonstrate that the arterial tissue remains in a viable state after 24 h of perfusion, which is crucial to perform biological time-lapse experiments with the perfusion system.

3.2 Confocal Scans

Figure 3 serves to visualize the confocal imaging and the receptor targeting concepts and shows two scans of an embedded aorta. Figure 3(c) shows a cross-section through the PDMS embedded aorta, containing an atherosclerotic plaque (yellow-pink freckles). The endothelium (orange) forms the border towards the lumen, which is filled with medium containing aptamer-Cy5 (coils with pink heads). Aptamer-Cy5 passively diffuses to the subendothelial space, where it is bound by intra-plaque macrophages via scavenger receptor A1. The sketch in Fig. 3(d) shows a macrophage with three surface bound aptamer-Cy5 molecules. The inset shows a macrophage that was stained with artificially perfused aptamer-Cy5 and imaged after tissue sectioning. The focal slice from confocal imaging [flat black rectangle in Fig. 3(c)] produces the fluorescent image, whereas the transmitted light reproduces the tissue contours, as illustrated by the sketches in Fig. 3(e) and 3(a), respectively. Figure 3(b) and 3(f) are transmitted light and confocal images from an aortic sample.

3.3 Macrophage Receptor Targeting

As a model to demonstrate the ability of our setup to perform biological perfusate mediated receptor targeting and imaging time-lapse experiments, we chose an aptamer-Cy5 construct as a ligand and the scavenger receptor A1 (SRA1) as the target.
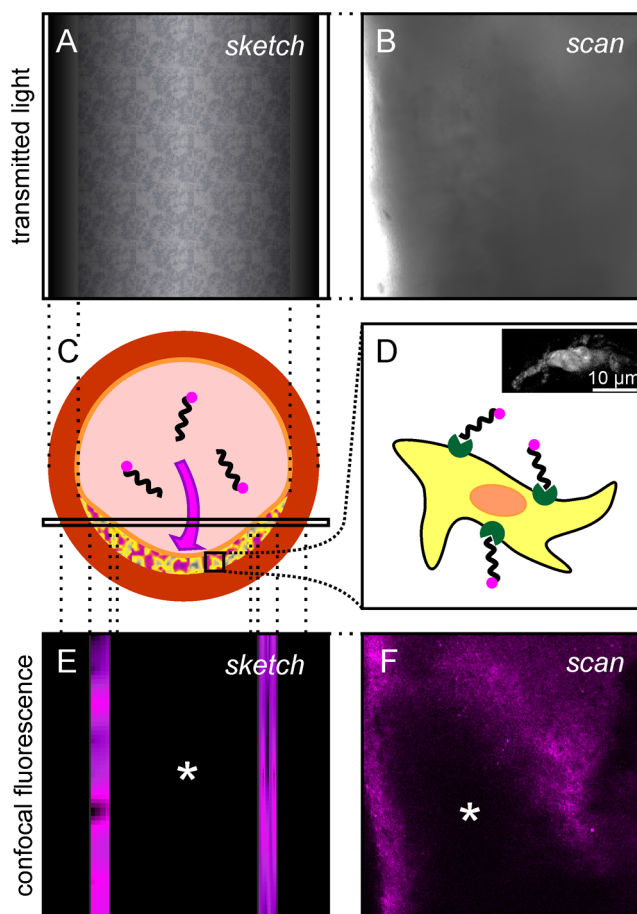

Fig. 3 Confocal imaging overview. (c) Schematic cross-section through the aorta containing a plaque. Coils with pink dots represent aptamer-Cy5. The black rectangle depicts the focal plane of the confocal microscope. In (e) and (a), fluorescence and transmitted signal, respectively, are shown schematically. In (b) and (b), real fluorescence and transmitted signal images are shown. (d) Schematic representation of a macrophage, with aptamer-Cy5 (coils with pink dots) bound to its scavenger A1 receptors (green). The inset shows the fluorescent signal of an intra-plaque macrophage, generated by the binding of circulating aptamer-Cy5. The image was acquired from a post-perfusion tissue section. The asterisk in (e) and (f) indicates the vessel lumen.

The scavenger receptor A1 belongs to the family of endocytic pattern recognition receptors. It promotes intracellular signaling, as well as the attachment, engulfment, and digestion of pathogens.[18] It is expressed by intra-plaque macrophages,[19] leading to oxidized-LDL uptake and the formation of foam cells (lipid laden macrophages). A first experiment was designed to determine the saturation kinetics of aptamer-Cy5 in plaque tissue, as reported by its fluorescent signal. We chose positions on the aorta containing either plaque or no plaque (as negative control) to be repeatedly laser-scanned. The scanning interval was set to 10 min, and the experiment duration was set to 20 h. After the first scanning cycle, perfusion of the aorta with cell culture medium containing 0.5 μM aptamer-Cy5 was initiated. After the experiment, the mean fluorescence intensities of selected regions of interest inside and outside plaques were plotted over time (results not shown). The resulting curves showed a saturation behavior, reaching a plateau after ~2 h. Therefore, we devised the next experiment to initiate with a 2-h incubation step with 0.5 μM aptamer-Cy5 in cell culture medium, followed by a 22-h washout step with pure medium. Between the two
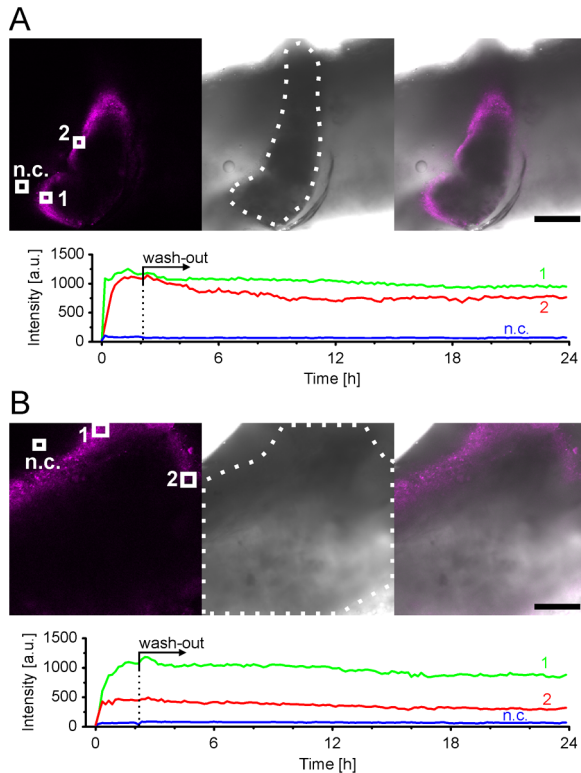
Fig. 4 Time-lapse confocal imaging. (a) and (b) Time-lapse experiment with aptamer-Cy5. Aptamer-Cy5 was circulated for 2 h, followed by a washout period for 22 h with cell culture medium. (a) and (b) represent two different positions on the aorta. Images from left to right are: aptamer-Cy5, transmitted light (the dotted lines indicate the plaque), merged. On each position, three regions of interest are defined: two within the plaque and one outside it. The mean fluorescent signal intensity of these regions is plotted over time. While negative control produces only a minor signal, on-plaque signal saturates rapidly and reaches a second plateau during the washout period. The scale bar in the images is 200 μm.

steps, the entire circulation tubing, including the aorta, was rinsed with medium. The resulting time-plots of the mean fluorescence signal over plaque areas during the incubation step showed similar behavior as in the preceding experiment. In the washout step, after minor reduction, the signal reaches a second plateau. The nonplaque areas, serving as negative controls, only produce a weak signal after the incubation step. In the washout step, this signal decreases almost to background level (i.e., the signal intensity before perfusion with aptamer-Cy5). These results are depicted in Fig. 4. Confocal laser scans of two separate positions on the same aorta, each separated into the fluorescent signal from aptamer-Cy5, the transmitted light, and the merging of these two images are displayed. On each of these two scans, three regions of interest were chosen, two within the plaque (named 1 and 2) and one outside it (named n.c. for negative control), resulting in three mean fluorescence signal curves over time.

3.4 Co-Localization of Receptor Targeting Signals

Figure 5(a) shows tissue sections of the mouse aorta that was used for the 24-h *ex vivo* perfusion experiment described in the paragraph above. In bright-field microscopy, the structure of the plaque can be distinguished from the physiological histological appearance of mouse aortas, i.e., there is an intra-luminal protrusion with increased granularity and disturbed elastin and collagen fiber continuity. In order to confirm the presence of a plaque, we used Bodipy lipid staining. Bodipy is a lipophilic fluorescent dye commonly used to stain lipid accumulations in histological specimens. In atherosclerotic plaques, intracellular lipid droplets (in foam cells) and extracellular lipid accumulations (necrotic lipid cores in advanced-stage atherosclerotic plaques) become stained. In our tissue section, the signal generated by the Bodipy staining spatially conforms to the protrusion observed in the bright-field, thus confirming the presence of atherosclerotic plaque tissue. Also, the fluorescent signal generated by aptamer-Cy5 is highly colocalized with the Bodipy signal. This proves that the enrichment of aptamer-Cy5 occurs in plaque tissue.
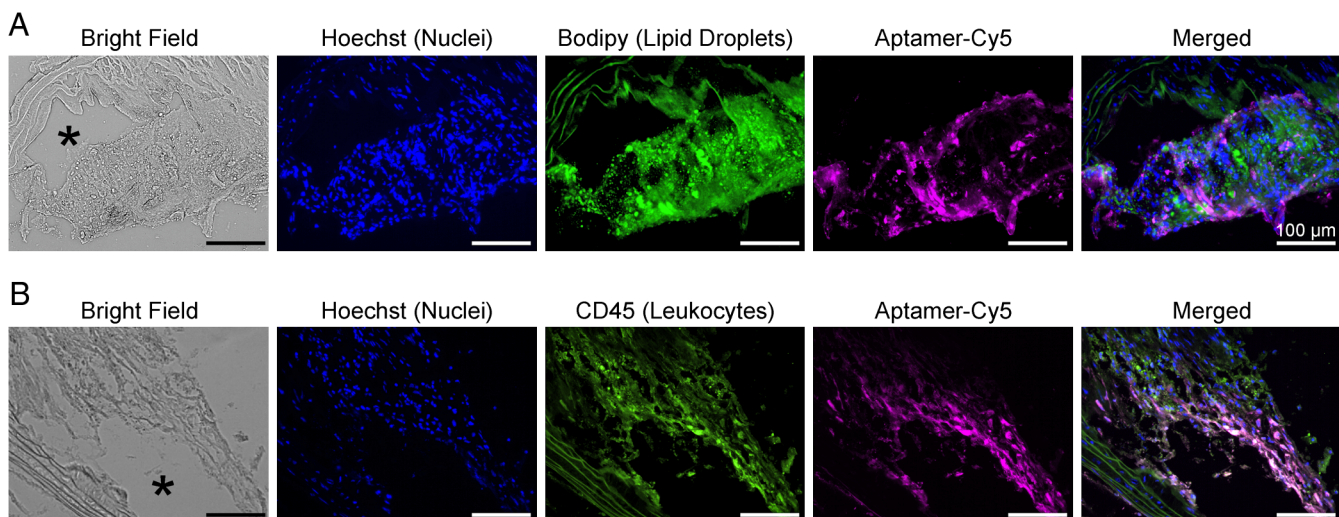

Fig. 5 Co-localization assays from *ex vivo* experiments. Mouse aorta tissue sections after *ex vivo* aptamer-Cy5 perfusion for 2 h, followed by a 22-h washout. The asterisk indicates the vessel lumen. (a) Co-localization of the aptamer-Cy5 signal with the Bodipy lipid staining. (b) Co-localization of the aptamer-Cy5 signal with the leukocyte marker CD45. These data indicate intra-plaque, leukocyte-specific localization of aptamer-Cy5.

We then wanted to test whether the aptamer-Cy5 inside the plaques is bound to leucocytes. The plaque sections were treated with an antibody for CD45, which is a membrane protein present on leucocytes. Fluorescent imaging revealed a high co-localization of the CD45 signal with the aptamer-Cy5 signal, with the signals localizing to single cells. This confirms specific binding of aptamer-Cy5 to leucocytes.

3.5 *In vivo Comparison Experiments*

In order to corroborate the biological validity of the data generated with the novel *ex vivo* model, we performed classical (i.e., one endpoint per animal after sacrificing) *in vivo* experiments as a reference. To this purpose, apoE$^{(-/-)}$ mice were treated by intravenous injection of aptamer-Cy5 in PBS to reach a blood concentration of ~1.5 μM. After 24 h, the mice were sacrificed, and the aortas were harvested, fixed, and cryosectioned. Tissue sections were processed and stained in identical manner as the sections from the *ex vivo* experiments. Imaging of these *in vivo* sections revealed co-localization of the aptamer-Cy5 signal with the Bodipy and the CD45 signal (Fig. 6). These *in vivo* results are in accordance with the *ex vivo* results and therefore corroborate the suitability of the *ex vivo* model for biological experiments.

4   Discussion

In this publication, we present a novel *ex vivo* mouse aorta perfusion platform. We tested the capabilities of this *ex vivo* model in terms of midterm (24 h) tissue viability and cell-specific targeting by a perfused compound, and we compared it to corresponding *in vivo* experiments. The successful implementation of the model enables *ex vivo* mouse aorta culture, treatment, and imaging by confocal time-lapse microscopy. Post-experimental tissue re-embedding and sectioning for histological staining and analysis is possible. The model is therefore potentially suitable for the investigation of vascular physiology, pathophysiology, and pharmacology. However, more exacting studies may be needed before the model can be utilized routinely.

The advantages of the model as compared to classical *in vivo* experiments are multiple endpoint generation (saving animals, as *in vivo* experiments require one animal per endpoint); less animal suffering due to investigation of novel compounds; fewer experimental variations due to variations of animal body weight, blood volume, and systemic clearance (by spleen, liver, and kidney); the ability to control the exact composition of the perfusate; and the ability to change rapidly the composition of the perfusate (e.g., for dynamic studies).

Compared to published mouse carotid artery *ex vivo* perfusion models,[10,11] the aorta perfusion model offers several advantages. First, the aorta contains larger and multiple atherosclerotic lesions at different stages,[6,20] and therefore offers more and statistically stronger data from one experiment. Second, classical *in vivo* experiments mostly utilize analysis of aortic plaques.[21] Usually, the aortic root is sectioned, and the plaque area and composition are measured. Also, the plaque area of the aortic arch or the entire aorta is measured by *en face* analysis, optionally with re-embedding and sectioning for further analysis. The aortic root is widely utilized, as it was the only location to develop atherosclerotic lesions in C57BL/6 mice upon fat feeding before the introduction of genetically modified mice as atherosclerosis models, such as the apoE$^{(-/-)}$ mouse.[7] In our model, the aortic root cannot be analyzed due to catheter insertion and ligation. Although earlier studies showed a close correlation between plaques in the aortic root and the entire aorta,[22] more recent studies found differences in behavior of aortic root plaques as compared to the plaques in the entire aorta.[23,24] Getz et al. proposed histological and immunochemical analysis of the innominate artery and the aortic arch as the "gold standard" in 2001.[25] However, in 2004, they proposed the innominate artery, left common carotid, and left subclavian branches of the aorta, as they might mimic more closely the plaques found in human carotid bifurcation.[12] The innominate artery in mice is the only lesion site to reproducibly develop intra-plaque thrombosis, although without formation of a thrombus, opposed to the situation in the human body.[26] It remains unclear which lesion sites in mice correspond best to lesion sites in humans, such as coronary arteries and carotid bifurcations. The plaque pathobiology in both humans and mice depends on the location within the arterial tree[12,13] and the local flow conditions,[27,28] complicating the comparison of different lesion sites. Also, the blood
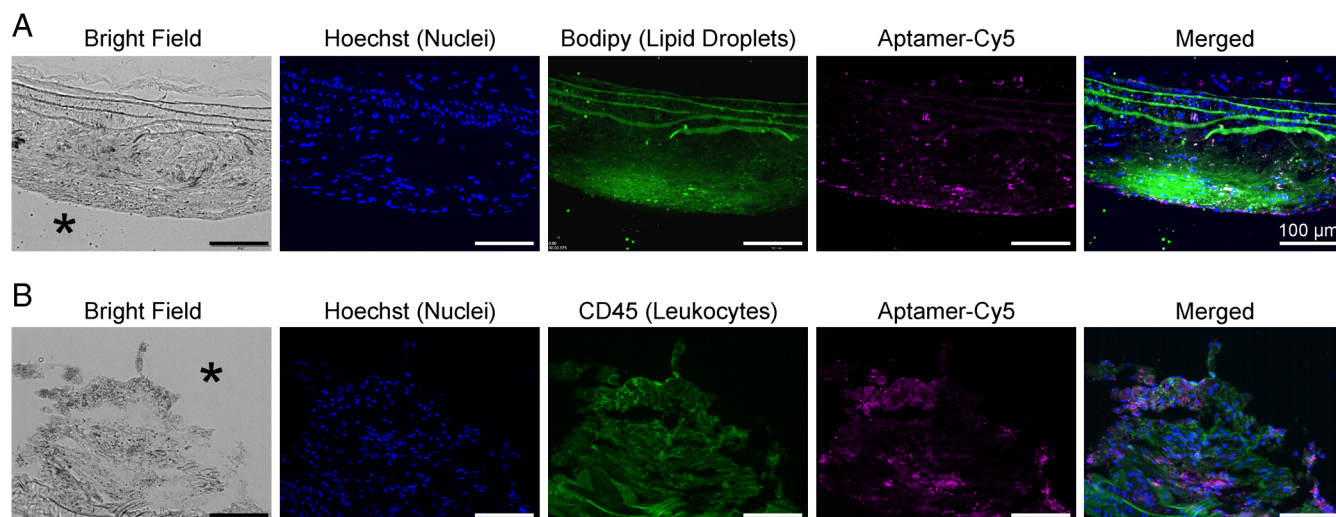

Fig. 6 Co-localization assays from *in vivo* experiments. Mouse aorta tissue sections after *in vivo* application of aptamer-Cy5. The asterisk indicates the vessel lumen. (a) Co-localization of the aptamer-Cy5 signal with the Bodipy lipid staining. (b) Co-localization of the leukocyte marker CD45 with the aptamer-Cy5 signal, confirming specific targeting of the leukocyte population inside plaques.

flow parameters and the biology of lesions, which includes the immune system, behave differently in mice than in humans.[8,15,29] However, a major advantage of our model lies in the direct comparability with existing data from classical *in vivo* experiments that utilized analysis of plaques within the aortic arch or the entire aorta. This is not straightforward with analysis of carotid plaques, as the pathobiology of the plaques differs depending on its location within the arterial tree and the local flow conditions, as stated above. Also, the correlation of vasa vasorum neo-vascularization with lesion formation can differ between the carotid artery and the aorta.[30]

Ex vivo models of mouse arteries used the suspension of arterial segments in a liquid environment. This allowed undisturbed pulse-induced elastic distension of the vessel. However, higher-magnification microscopy for subcellular resolution can be hindered due to motion artifacts. A freely suspended aortic arch would be especially prone to shifting and motion artifacts, due to its geometry. The embedding of the aorta in the PDMS matrix obviates these issues.

Intravital microscopy of mouse arteries has been performed with the abdominal aorta, cremaster arterioles, common carotid artery, and others for the study of various biological phenomena. For the study of atherosclerosis, the common carotid artery was intravitally imaged with confocal[31] and two-photon[32] microscopy. Intravital microscopy offers the advantage of multiple endpoints within one experiment under almost physiological conditions. However, its major limitation is its experimental duration limitation to maximal anesthesia duration, although anesthesia durations of up to 6.5 h with survival of the mice have been reported.[33] Also, it is "extremely challenging" to perform[32] and requires dedicated instrumentation and continuous observation. Humidified isoflurane inhalation was used for anesthesia, partly together with external artificial ventilation of the lungs. Intravenous infusion was applied to pertain the liquid balance. Furthermore, body temperature, arterial blood pressure, and respiration were monitored, with the animal lying on a warming plate to maintain physiological body temperature. Due to motion artifacts, only low-resolution imaging was possible in one study.[31] In order to reduce motion artifacts and allow subcellular resolution, heart pulse and respiration triggered imaging was applied in another study.[34]

As to the perfusion parameters in intravital microscopy, the heart rate and the relative composition of the blood can be modulated pharmacologically, by (partial) ligation, and by infusion of liquids, but they cannot be controlled to the extent and with the dynamic speed and accuracy of *ex vivo* perfusion models. Also, it was observed that the surgical procedure involved to expose the artery can induce changes in endothelial activity.[35]

An epi-fluorescence approach, utilizing glass fibers and a sensor unit attached to the skull of a mouse, which allows free movement of animals to study brain neuron activity and microcirculation, has been demonstrated.[36] However, this requires specialized knowledge and dedicated instrumentation, and it is limited to organs where fixation of the signal acquisition unit is possible.

Two-photon microscopy,[37,38] as compared to confocal microscopy, offers advantages such as improved spatial resolution at greater depths and reduced photo-damage. However, the instrumentation is costly and not yet widespread. In our experiments, with confocal microscopy, we achieved a sufficient penetration depth with reasonable image quality. Therefore, we believe that confocal microscopy, as applied in our *ex vivo* model, offers a good compromise between the availability of the instrumentation and the quality of the acquired images. Nevertheless, our model is also suitable for two-photon imaging as tested for the excitation of DAPI (4′,6-diamidino-2-phenylindole) at 850 nm in a PDMS-embedded aorta (data not shown).

A difference of the presented aorta *ex vivo* model from *in vivo* conditions is the reduced pulse rate and probably also the different pulse curve of the peristaltic pump, as compared to the physiological heart rate and aortic pulse curve of mice. This can have an influence on the atherosclerotic lesions, mediated by endothelial cells, due to the changed flow conditions. We observed reduced deposition of aptamer-Cy5 in the plaques when we perfused the aorta *ex vivo* under continuous flow with a syringe pump as compared with peristaltic pumping. The flow and pressure dependence of subendothelial particle deposition in pig common carotid arteries has been described.[39] The use of a dedicated pump could reduce the differences between physiological and artificial pulse curves.

Another potential difference from *in vivo* conditions may be the reduction of elastic vessel distension due to the additional elastic force induced by the PDMS matrix.

Furthermore, the draining lymph vessels from adventitial lymphatic tissue located adjacent to the plaques,[4,40] and the venules of the vasa vasorum (also the intra-plaque neo-vascularization[35]), probably become occluded due to the PDMS embedding. However, the isolation of the adventitial immunologic tissue also occurs with liquid immersion *ex vivo* models and probably also with intravital microscopy. It is not evident what the consequences are on plaque pathobiology within days (for example, during time-lapse experiments).

Extending the experimental duration beyond 24 h may require adaptation of the circulating medium for optimal endothelial cell culture (e.g., the addition of growth factors), as this is the most sensitive vascular wall cell type. However, we believe that *ex vivo* culture up to several days can be achieved using this method, opening windows of opportunity for long-term biological experiments.

For the future, we plan to increase the spatial microscopical resolution to enable subcellular imaging, extend the *ex vivo* experimental duration, test novel targeting compounds, and study pharmacological interventions.

References

1. V. L. Roger et al., "Heart disease and stroke statistics—2012 update: a report from the American Heart Association," *Circulation* **125**(1), e2–e220 (2012).
2. A. D. Lopez et al., "Global and regional burden of disease and risk factors, 2001: systematic analysis of population health data," *Lancet* **367**(9524), 1747–1757 (2006).
3. G. K. Hansson and A. Hermansson, "The immune system in atherosclerosis," *Nature Immunol.* **12**(3), 204–212 (2011).
4. E. Galkina and K. Ley, "Immune and inflammatory mechanisms of atherosclerosis (*)," *Ann. Rev. Immunol.* **27**, 165–197 (2009).

5. C. Weber and H. Noels, "Atherosclerosis: current pathogenesis and therapeutic options," *Nat. Med.* **17**(11), 1410–1422 (2011).

6. J. J. Chiu and S. Chien, "Effects of disturbed flow on vascular endothelium: pathophysiological basis and clinical perspectives," *Physiol. Rev.* **91**(1), 327–387 (2011).

7. A. S. Plump et al., "Severe hypercholesterolemia and atherosclerosis in apolipoprotein E-deficient mice created by homologous recombination in ES," *cells* **71**(2), 343–353 (1992).

8. J. F. Bentzon and E. Falk, "Atherosclerotic lesions in mouse and man: is it the same disease?" *Curr. Opin. Lipidol.* **21**(5), 434–340 (2010).

9. C. L. Ramos et al., "Direct demonstration of P-selectin- and VCAM-1-dependent mononuclear cell rolling in early atherosclerotic lesions of apolipoprotein E-deficient mice," *Circ. Res.* **84**(11), 1237–1244 (1999).

10. M. van Zandvoort et al., "Two-photon microscopy for imaging of the (atherosclerotic) vascular wall: a proof of concept study," *J. Vasc. Res.* **41**(1), 54–63 (2004).

11. R. T. Megens et al., "Two-photon microscopy of vital murine elastic and muscular arteries. Combined structural and functional imaging with subcellular resolution," *J. Vasc. Res.* **44**(2), 87–98 (2007).

12. P. A. VanderLaan, C. A. Reardon, and G. S. Getz, "Site specificity of atherosclerosis: site-selective responses to atherosclerotic modulators," *Arterioscler. Thromb. Vasc. Biol.* **24**(1), 12–22 (2004).

13. J. T. Chi et al., "Endothelial cell diversity revealed by global expression profiling," *PNAS* **100**(19), 10623–10628 (2003).

14. P. C. Thomas, S. R. Raghavan, and S. P. Forry, "Regulating oxygen levels in a microfluidic device," *Anal. Chem.* **83**(22), 8821–8824 (2011).

15. S. P. Forry and L. E. Locascio, "On-chip CO_2 control for microfluidic cell culture," *Lab Chip.* **11**(23), 4041–4046 (2011).

16. J. Suo et al., "Hemodynamic shear stresses in mouse aortas: implications for atherogenesis," *Arterioscler. Thromb. Vasc. Biol.* **27**(2), 346–351 (2006).

17. Y. Nakashima et al., "Upregulation of VCAM-1 and ICAM-1 at atherosclerosis-prone sites on the endothelium in the ApoE-deficient mouse," *Arterioscler. Thromb. Vasc. Biol.* **18**(5), 842–851 (1998).

18. M. Krieger and J. Herz, "Structures and functions of multiligand lipoprotein receptors: macrophage scavenger receptors and LDL receptor-related protein (LRP)," *Ann. Rev. Biochem.* **63**, 601–637 (1994).

19. A. Matsumoto et al., "Human macrophage scavenger receptors: primary structure, expression, and localization in atherosclerotic lesions," *PNAS* **87**(23), 9133–9137 (1990).

20. Y. Nakashima et al., "ApoE-deficient mice develop lesions of all phases of atherosclerosis throughout the arterial tree," *Arterioscler. Thromb.* **14**(1), 133–140 (1994).

21. S. C. Whitman, "A practical approach to using mice in atherosclerosis research," *Clin Biochem Rev.* **25**(1), 81–93 (2004).

22. R. K. Tangirala, E. M. Rubin, and W. Palinski, "Quantitation of atherosclerosis in murine models: correlation between lesions in the aortic origin and in the entire aorta, and differences in the extent of lesions between sexes in LDL receptor-deficient and apolipoprotein E-deficient mice," *J. Lipid Res.* **36**(11), 2320–2328 (1995).

23. P. K. Witting et al., "Site-specific antiatherogenic effect of probucol in apolipoprotein E-deficient mice," *Arterioscler. Thromb. Vasc. Biol.* **20**(8), e26–e33 (2000).

24. P. Chew et al., "Site-specific antiatherogenic effect of the antioxidant ebselen in the diabetic apolipoprotein E-deficient mouse," *Arterioscler. Thromb. Vasc. Biol.* **29**(6), 823–830 (2009).

25. C. A. Reardon and G. S. Getz, "Mouse models of atherosclerosis," *Curr. Opin. Lipidol.* **12**(2), 167–173 (2001).

26. M. E. Rosenfeld et al., "Progression and disruption of advanced atherosclerotic plaques in murine models," *Curr. Drug Targets.* **9**(3), 210–216 (2008).

27. C. Cheng et al., "Atherosclerotic lesion size and vulnerability are determined by patterns of fluid shear stress," *Circulation* **113**(23), 2744–2753 (2006).

28. P. F. Davies, "Hemodynamic shear stress and the endothelium in cardiovascular pathophysiology," *Nat. Clin. Pract. Cardiovasc. Med.* **6**(1), 16–26 (2008).

29. P. Libby, P. M. Ridker, and G. K. Hansson, "Progress and challenges in translating the biology of atherosclerosis," *Nature* **473**(7347), 317–325 (2011).

30. A. C. Langheinrich et al., "Vasa vasorum neovascularization and lesion distribution among different vascular beds in ApoE$^{-/-}$/LDL$^{-/-}$ double knockout mice," *Atherosclerosis* **191**(1), 73–81 (2007).

31. A. N. Pande et al., "Detection of macrophage activity in vivo using multichannel, high-resolution laser scanning fluorescence microscopy," *J. Biomed. Opt.* **11**(2), 021009 (2006).

32. W. Yu et al., "In vivo imaging of atherosclerotic plaques in apolipoprotein E deficient mice using nonlinear microscopy," *J. Biomed. Opt.* **12**(5), 054008 (2007).

33. G. Szczesny et al., "Long-term anaesthesia using inhalatory isoflurane in different strains of mice-the haemodynamic effects," *Lab. Anim.* **38**(1), 64–69 (2004).

34. R. T. Megens et al., "In vivo high-resolution structural imaging of large arteries in small rodents using two-photon laser scanning microscopy," *J. Biomed. Opt.* **15**(1), 011108 (2010).

35. E. E. Eriksson, "Intravital microscopy on atherosclerosis in apolipoprotein e-deficient mice establishes microvessels as major entry pathways for leukocytes to advanced lesions," *Circulation* **124**(19), 2129–2138 (2011).

36. B. A. Flusberg et al., "High-speed, miniaturized fluorescence microscopy in freely moving mice," *Nat Methods* **5**(11), 935–938 (2008).

37. W. Denk, J. H. Strickler, and W. W. Webb, "Two-photon laser scanning fluorescence microscopy," *Science* **248**(4951), 73–76 (1990).

38. F. Helmchen and W. Denk, "Deep tissue two-photon microscopy," *Nat. Methods* **2**(12), 932–940 (2005).

39. N. C. Chesler and O. C. Enyinna, "Particle deposition in arteries ex vivo: effects of pressure, flow, and waveform," *J. Biomech. Eng.* **125**(3), 389–394 (2003).

40. M. P. Moos et al., "The lamina adventitia is the major site of immune cell accumulation in standard chow-fed apolipoprotein E-deficient mice," *Arterioscler. Thromb. Vasc. Biol.* **25**(11), 2386–2391 (2005).